THE JOURNAL OF PHYSICAL CHEMISTRY A

pubs.acs.org/JPCA Article

On the Formation of Interstellar CH^- Anions: Exploring Mechanism and Rates for CH_2 Reacting with H^-

E. Yurtsever, M. Satta, R. Wester, and F. A. Gianturco*

Cite This: *J. Phys. Chem. A* 2020, 124, 5098–5108 Read Online

ACCESS | Metrics & More | Article Recommendations

ABSTRACT: We present accurate ab initio calculations on the structural properties of a gas-phase reaction of possible interest for Saturn's outer atmosphere chemistry, in which the CH_2 molecule has been detected. In the present study, that molecule is made to react with the H^- anion to form the CH^- species, one considered as a possible intermediate in ionic processes networks. The results indicate that this reaction is markedly exothermic and proceeds with the formation of an intermediate, which occurs via only a shallow barrier below the reagents and progresses directly to the product region. The corresponding rate coefficients of reactions are also computed by making use of the variational transition state theory modeling and found to efficiently lead to the formation of the final anion even at the lower temperatures of interstellar medium conditions.

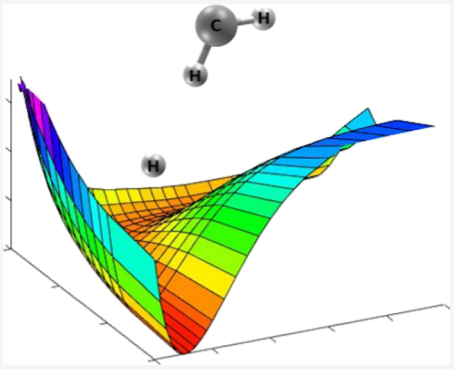

1. INTRODUCTION

Over the last 50 years, the formation of interstellar anions and their likely detection have been an important topic for the astrochemistry community, starting with Dalgarno and McCray[1] who for the first time explored the role of anions, specifically H^-, O^-, C^-, CH^-, C_2H^-, CN^-, and S^-, in the formation of simple molecules in interstellar clouds. They concluded at the time that interstellar anions were scarce and their contribution to the formation of other molecular species would not be very significant. These results were attributed to the relatively slow rate of formation found from their modeling of radiative electron attachment (REA): $\approx 10^{-15}$ cm^3 s^{-1} $molecule^{-1}$ was in fact the average value found by their early calculations. However, a few years later, based on a simple statistical model, Herbst[2] suggested that anions could be efficiently formed in dense interstellar clouds. He showed from his own modeling that for large neutral species with large electron affinity (EA; C_4H, C_3N, C_5N, C_9N, etc.), the radiative attachment rate could be near to the collision limit $\approx 10^{-7}$ cm^3 s^{-1} $molecule^{-1}$. One of the most relevant results of this work was the prediction of an anion-to-neutral ratio between 1 and 10%, which was later corroborated by new astronomical observations. Further calculations with a more sophisticated scattering model were carried out in our group[3] and found the REA rates for C-rich chains, albeit smaller than those found earlier by Herbst, to be $\approx 10^{-9}$ cm^3 s^{-1} $molecule^{-1}$. Finally, the definite observational proof that anions could exist in interstellar medium (ISM) came in 2006, when McCarthy et al.[4] detected for the first time C_6H^- in the circumstellar envelope IRC+10216 and the dark cloud TMC-1. The anion-to-neutral ratios were in an agreement with the early predictions of Herbst, 1−5% for IRC+10216 and 2.5% for TMC-1, thus supporting the hypothesis that anions could be efficiently synthesized in the ISM by REA or by some other chemical route. The detection of C_6H^- led to the subsequent detection of five other anions, namely, C_4H^-, C_8H^-, CN^-, C_3N^-, and C_5N^-, in a variety of interstellar sources.[5−9] These observations gave rise quickly to new chemical modeling for the interstellar sources where the anions had been detected as well as of other likely sources of anionic molecules.[10−12] These models yielded anion-to-neutral ratios that were reasonably successful at reproducing observations for the largest anions (C_6H^-, C_8H^-, and C_7N^-) and less successful for smallest anions (CN^-, C_4H^-, and C_3N^-), leading to the preliminary conclusion that RA processes would be markedly less efficient for molecules with few degrees of freedom. Further experimental studies carried out earlier in our group[13,14] on the efficiency of photodetachment mechanisms for the destruction of C-bearing and N-bearing molecular anions have provided clear evidence on the likely importance of starlight in driving their destructions outside chemical networks. Furthermore, the extended investigations of possible mechanisms of formation involving chemical reactions with

Received: March 18, 2020
Revised: May 27, 2020
Published: May 28, 2020

https://dx.doi.org/10.1021/acs.jpca.0c02412
J. Phys. Chem. A 2020, 124, 5098–5108

other, simpler and reasonably abundant atomic species such as H, O, N, and C, have provided additional laboratory data on chemical processes, which could play a role in the formation of a variety of smaller anions, some of them different from those of the earlier observations but still often predicted to be at border-line values of observable column densities.[12,15,16]

A case in point is that of the formation of CH^- from an initial neutral−ion reaction of CH_2 with H^-, which will be the main object of study in the present work. Methylene, CH_2, as the prototypical carbene, is one of the most studied of all reactive intermediates, while the chemistry of its anion, CH_2^- is still almost completely unknown. Early spectroscopic work established the existence of two low lying electronic states: the ground X^3B_1 state and the excited a^1A_1 state. Subsequent spectroscopic studies of the visible electronic band system $b^1B_1 \leftarrow a^1A_1$ lead to an accurate characterization of the molecule in the a^1A_1 state, but for many years, the ground state structure was uncertain.[17,18]

The astrochemical models dealing with anions in experiments at room temperature[19,20] included the expected formation of C_2H^- from reactions with e^- with several C-rich molecules but never were able to produce or observe CH^- among the anionic products. As a matter of fact, the product CH^- has been considered as a possible reaction intermediate[19] but never actually observed or produced in laboratory reactions at room temperature. It thus appears that the abundance of CH^- in cold clouds is likely to be very small,[19,20] while the presence of CH_2 has been found in the atmosphere of Titan, where CH_2^- has also been found as a anionic partner.[21] These observations and modeling of the anion chemistry in the outer atmosphere of Titan, Saturn's largest moon, are thus indicating that with the additional suggestion of the possible presence of the H^- partner as an anion,[21] it stands to reason to investigate the possible efficiency of the latter neutral radical to form the yet unobserved CH^- species through an ionic chemical reaction that could easily be another component to be employed in the chemical network for that atmosphere.

In the present study, we therefore shall make a close observation from computational methods of the general structural features of this simple reaction and then decide from our finding what would be the most realistic model to employ to obtain the reaction rates, which may be in turn included in more extended evolutionary simulations of molecular abundances in diffuse molecular clouds[22] or, even more realistically, to describe their role on the chemistry of Titan's atmosphere.[21] The first details from calculations will be of course those that can help us to establish the general energetics of the present reaction

$$CH_2(^3B_1) + H^-(^1S) \rightarrow CH^-(^3\Sigma) + H_2(^1\Sigma) \quad (1)$$

in order to define more specifically, and as realistically as possible, its enthalpy features via a vis those discussed in the general literature.[23−25] The following section will therefore present the details of the calculations and shall start to outline the possible mechanism for the formation of CH^- from reaction 1.

It is also interesting to note that a competing destruction mechanism could also be considered for the reaction above

$$CH_2(^3B_1) + H^-(^1S) \rightarrow CH_3(^2A_1) + e^- \quad (2)$$

which describes the formation of another neutral molecule, the methyl radical, through an associative detachment mechanism. The latter reaction has an estimated exothermicity of around 3.0 eV and has only been considered in earlier chemical models through its standard Langevin rate coefficients[26] which were estimated to be around $\approx 10^{-9}$ cm^3 s^{-1} molecule^{-1}, so very little is actually known about its structural details. It will not be further considered in the present work, which will mainly focus on the chemical mechanism of eq 1.

2. COMPUTATIONAL DETAILS

Calculations were carried out with different choices of post-Hartree−Fock ab initio methods. Initial analysis dealt with all of the molecular species involved to be fully optimized using the coupled-cluster method with full treatment of singles and doubles and an iterative treatment of triples: CCSD(T) as implemented in the MOLPRO suite of codes.[27] The basis set is chosen to be aug-cc-pVTZ for the reasons explained below in the data of Table 1. The zero-point-energy (ZPE) corrections were included in all of the calculations. The evaluation of the potential energy curves and surfaces was carried out with the same method and basis set, but using restricted optimizations in order to follow in turn several and different possible reaction paths. The details of these optimizations are given in the discussion below for each set of calculations. The calculations were also carried out with the density functional theory (DFT), employing the B3LYP/6−311++G** expansion level, as described in the Gaussian set of codes,[28] to generate the dense grid of points required by the calculations of the reaction rates within the variational transition state (TS) theory (VTST) approach (see further details below). The results from the present CCSD(T) calculations are reported by the data detailed in the columns of Table 1. We shall further discuss later the outcomes from DFT calculations, which have to be used for the VTST reaction rates (see below) as they are also providing rather good accord with the results listed in Table 1. We would also like to point out here that the DFT results are not used to evaluate energy positions [data obtained instead via the more accurate CCSD(T) methods] but only to give the complex's geometries and vibrational frequencies for the partition functions as described in the next section.

Table 1. Computed CCSD(T) Energetics of the Involved Reactants and Expected Products[a]

	aug-cc-pVTZ		aug-cc-pVQZ	
	energy	ZPE corrected energy	energy	ZPE corrected energy
CH^-	−38.455214	−38.449448	−38.462676	−38.456869
H_2	−1.172636	−1.162908	−1.173867	−1.164141
CH_2	−39.080072	−39.063308	−39.088071	−39.071263
H^-	−0.526562	−0.526562	−0.527139	−0.527139
CH_3^-	−39.763245	−39.734900		
products	−39.627850	−39.612356	−39.636543	−39.621010
reactants	−39.606634	−39.589871	−39.615210	−39.598403
ΔE (eV)	−0.577	−0.612	−0.581	−0.615

[a]The total energies of reactants and products are calculated from sum of separate species. Total energies are in hartree. See main text for further discussion.

We see from these results that all the different levels of calculations indicate this reaction to be clearly exothermic, with the best agreement with the existing NIST data,[23] which indicate an exothermicity of 0.611 eV, being provided by the

https://dx.doi.org/10.1021/acs.jpca.0c02412
J. Phys. Chem. A 2020, 124, 5098−5108

CCSD(T) aug-cc-pVTZ results reported in both tables. The large differences in the EA values between the reacting anion H^- (0.74 eV) and the product of the electron transfer (ET) process CH^- (1.260 eV)[29] suggest strong reasons for the reaction's exothermicity. In terms of the most effective path of approach between reactants, to yield the products of reaction 1, we found that the attack from the H^- anion along one of the CH_2 bonds provides, as we will discuss more in detail below, the minimum energy path (MEP) to products, as shown by the simple geometry of Figure 1.

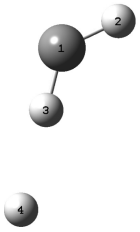

Figure 1. Reaction coordinates along the chosen path of minimum energy (see main text) and numbering of the atoms in the complex. The level of CCSD(T) calculation employed the -pVTZ basis set of Table 1.

The structural parameters of the individual molecular partners produced by our calculations are given in Table 2, where we also see that all calculated parameters are in good accord with their experimental counterparts reported in the last column of the same table.

Below, we further analyze in detail the energy dependence of a few, restricted configurations of the reaction partners in order to isolate what would be the most energetically efficient path to the present products. The results in Figure 2 describe the approach of the H^- (H4) anion to the H3−C bond, as shown by Figure 1. The calculations were carried out for every fixed H3−H4 distance, for which the C−H2, C−H3 distances and the H2−C−H3 angle are optimized with CCSD(T)-aug-cc-pVTZ calculations while the H4−H3−C fragment is kept linear. When the collinearity is not enforced, the optimization process switches the approaching H^- (H4) ion to the midpoint of the H2−H3 line.

The energy profile along the collinear approach indicates the exothermic behavior along that path, with a shallow local minimum in the region of the TS, followed by a very small local maximum before going into the products. The same level of calculations mentioned in the previous figures is employed here. An enlarged view is shown in Figure 3 below. The relative energetics of the features in Figure 3 are given more specifically by the additional calculations in Table 3.

The energy changes from the min1 to the max location is only of 4 meV, both configurations being well above the products at the min2 shown in Figure 2, and used as energy reference in Table 3. As the relative distance between the

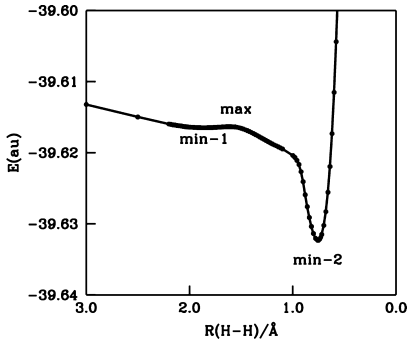

Figure 2. Computed, optimized total energy along the reaction path as a function of the approaching H^- partner. See main text for further details on the restricted path shown in this figure and on the level of CCSD(T) basis set employed.

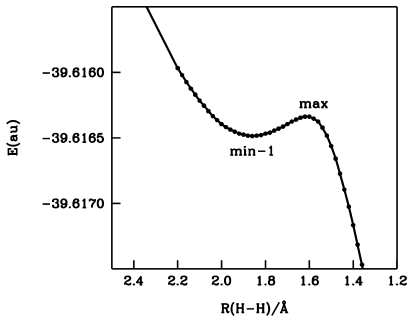

Figure 3. Enlarged view of the reaction energetics near the TS formation. See main text for further details.

approaching H^- anion (H4) decreases from the reactants down to the complex region, the minor energy change from min1 to the max geometries indicates the formation of TS structures before the ET process as the two H atoms form the neutral molecular hydrogen product. It is also interesting to note that both calculations at the MP2 and at the CI levels indicate a TS in the vicinity of the "max" geometry, while a fuller optimization without the linearity constraint of Figure 2 produces a TS configuration very close to the latter but with slightly different structural details. Its shape is shown in Figure 4 while the final geometry optimization of the TS is given in Table 4.

The above features indicate that the full TS configuration involves now two of the atoms (H4−H3) closer to each other, a slightly greater value of the molecular angle in the CH_2 component, and a marked elongation of the C−H3 bond, indicating the formation of the neutral H_2 product while the ET step of the reaction is also taking place, as further discussed below. Another interesting display of the energy behavior during the present reaction is shown by the data in Figure 5. We report the global energy optimization of the C−H bond of the initial CH_2 molecule as the latter is broken during the

Table 2. Structural Parameters of the Relevant Partners[a]

molecule	coordinate	CCSD(T)/aug-cc-pVTZ	CCSD(T)/aug-cc-pVQZ	Exp.[23]
CH^-	R(C−H)	1.139	1.137	1.12
H_2	R(H−H)	0.743	0.742	0.741
CH_2	R(C−H)	1.079	1.078	1.075
	θ(H−C−H)	133.7	133.7	133.8

[a]Distances in Å and angles in degrees.

https://dx.doi.org/10.1021/acs.jpca.0c02412
J. Phys. Chem. A 2020, 124, 5098−5108

Table 3. Computed Energetics and Geometries at the Points Along the Reaction Path Marked in Figures 2 and 3[a]

		total energy (hartree)		ΔE (meV)	
		aug-cc-pVTZ	aug-cc-pVQZ	aug-cc-pVTZ	aug-cc-pVQZ
reactants	$CH_2 + H^-$	−39.606634	−39.615210	699	701
min-1	R(H4−H3) = 1.86 Å	−39.616486	−39.625083	431	432
max	R(H4−H3) = 1.60 Å	−39.616341	−39.625020	435	434
min-2	R(H4−H3) = 0.76 Å	−39.632332	−39.640962	0	0
products	$CH^- + H_2$	−39.627850	−39.636543	122	120

[a]See main text for additional details.

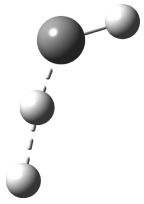

Figure 4. Detailed structure of the optimized TS configuration around the location of the "max" geometry in Figure 3. See main text for further details on the level of calculations employed here.

Table 4. Detailed Geometric Parameters and Charge Localization for the TS Complex from the Full Optimization of the Complex Around the Location of the "Max" Point of Figure 3[a]

	MP2	CI	max
R(H2−C)	1.105	1.113	1.101
R(C−H3)	1.230	1.300	1.142
R(H4−H3)	1.275	1.175	1.600
θ(H2−C−H3)	126.3	129.9	123.18
q(H4)	−0.723	−0.453	−0.852
Q(H2CH3)	−0.277	−0.547	−0.148

[a]The geometric details of the latter are also given in the last column on the right.

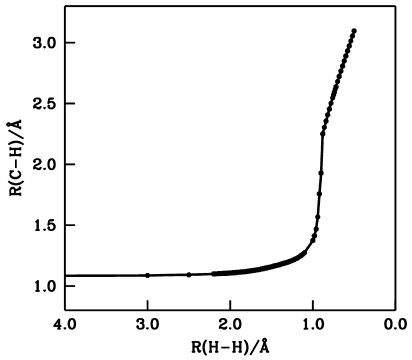

Figure 5. Minimum energy calculations as a function of the approaching H^- anion to the molecular partner [distance H4−H3, given as R(H−H) coordinate in the figure] while the bond involved in CH_2 (the C−H3 bond given as C−H in the figure) is broken to form the CH^- product. See main text for further discussion and for the type of basis set employed.

approach of the H^- anion to the molecular partner. One clearly sees that, until the approaching anionic atom reaches the geometry range describing the neutral H_2 molecule, the energy curve is essentially flat. After that point, the energy remains at its minimum while the involved C−H bond is broken and the residual CH^- fragment moves away. This ET step will be further discussed later.

We now look at the behavior of the initial molecular angle during the reaction with the data in Figure 6. What we show there is the minimum energy values of the complex as the CH_2 angle is varied while the H^- anion approaches the involved C−H bond (H4−H3 distance) in the molecule.

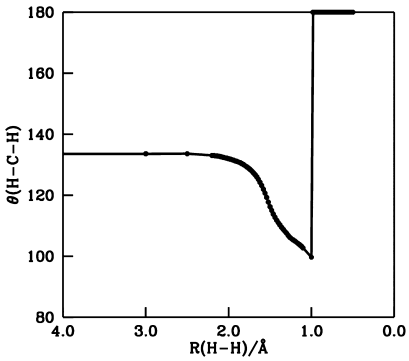

Figure 6. Energy minima calculated for the same process of Figure 5, this time involving the variations of the H2−C−H3 angle in the initial reagent (θ(H−C−H) coordinate) as the H anion approaches the molecular partner (R(H−H) coordinate in the figure). As the products $H_2 + CH^-$ are formed, (jump seen on the right) the previous angle has no more meaning as it could take any value. See main text for further details.

The data show clearly that little change occurs when the approaching anion remains far away (left side of the figure). Only when the two reacting H···H atoms are around 2 Å from each other the angle starts becoming smaller as the relative H···H distance reaches the ET region and the residual CH^- product (the distance C−H2) rapidly turns away from the neutral H_2 molecule by increasing the angle to 180°. Thus, the energy profiles of both Figures 5 and 6 indicate that the reactive mechanism occurs within a rather narrow range of relative geometries of the TS complex found by our calculations. To investigate where the actual ET step occurs, we report in Figure 7 the Mulliken charges as the reaction progresses along the H3−H4 path. What we see in Figure 7 is an initial ET mechanism around a relative distance of the H3−H4 bond whereby the excess negative charge is equally shared within the complex by the incoming H anion and the residual CH_2 fragment. This is also visible from the data reported by Table 3 where the TS geometry indicates the nearly equal sharing of the "hopping" electron between the H4 approaching atom and the CH_2 fragment (H2−C−H3 fragment). In contrast to this result, the geometry of the "max" configuration of Figure 2 shows a longer H4−H3 bond and the excess negative charge still largely on the approaching atomic anion

https://dx.doi.org/10.1021/acs.jpca.0c02412
J. Phys. Chem. A 2020, 124, 5098−5108

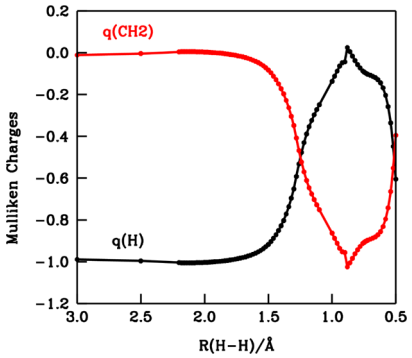

Figure 7. Variation of the excess negative charge location (Mulliken charges) along the reaction coordinate discussed in the earlier figures: the H4−H3 distance between reagents. The black line reports the charge variation on the H^- partner while the red line shows the same variation on the CH fragment. The initial partners on the left are the two reaction partners. More details in the main text.

(see again Table 4) thus indicates that the ET step has not yet occurred. The data in Figure 7 show that at the shorter distance between the H3 and H4 atoms in the "min2" configuration of Figures 2 and 3, the excess electron has fully moved on to the CH_2 fragment and has entirely left the approaching atomic anion. Thus, Figures 2 and 3 suggest the ET process to occur after the TS formation and on the way down the exothermic profile. This therefore explains the presence of two nearby minima in the behavior of the collinear path.

The reaction described by the behavior of its IRC is reported by Figure 8. The IRC, for example, see: ref 30, is an imaginary

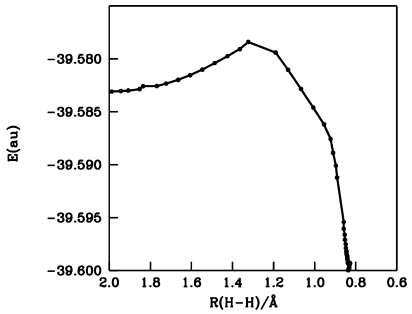

Figure 8. Total energy variation computed along the reaction's intrinsic reaction coordinate (IRC). This coordinate starts from the true TS. This TS connects reactants and products, where the left-hand asymptote corresponds to CH_2 and H^- (the reactants), while the right-hand asymptote is CH^- and H_2 (the products). The total energy values come here from the MP2 calculations (see the earlier discussion).

minimum energy trajectory, which passes through the TS and moves infinitely slowly. Its initial direction at the TS is given by the normal mode of imaginary frequency. In classical terms, such a trajectory satisfies the classical equations of motion, although at each step of the trajectory each component of the linear momentum P_j, and therefore of the kinetic energy, is set to zero.[31] At the TS (a saddle point), where the intrinsic reaction coordinate is to start, the gradient of the energy value taken from the RPES is zero so that the initial direction of the IRC is then determined by the direction of the normal coordinate that has a negative eigenvalue at that saddle point.

In Figure 8, we see that the positioning of the TS around the (H3−H4) distance located at the "max" configuration (the one discussed before) shows the presence of a shallow maximum and a marked energy descent into the product region on the right side of the curve. This behavior confirms the exothermic, barrierless reaction structure along its MEP.

In the three panels of Figure 9 we show possible reaction paths where the H^- anion approaches the CH_2 partner from

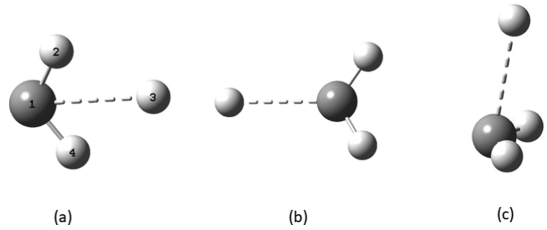

Figure 9. Three different, alternative paths of approach for the H^- partner into the CH_2 reacting molecule. See main text for further details.

different directions, that is, from left to right: (i) on the plane along the bisector of the molecular angle; (ii) still on the plane but from the C-atom side; (iii) perpendicularly to the molecular plane. A comparison of the energy variations along these three paths, as the H^- anion approaches the molecule (with full optimization of its bonds and angle), is reported by the curves in Figure 10.

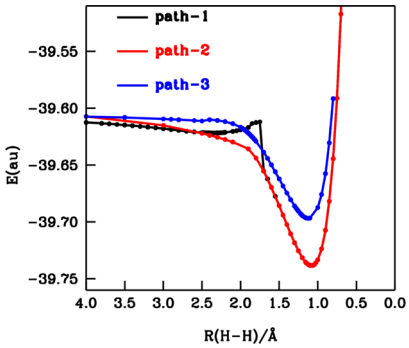

Figure 10. Variation of the total energy of the complex as a function of the R(H3−H4) distance for the different approaches of Figure 9. The numbering from 1 to 3 indicates the paths from left to right. At the jump location along path 1, the two other H atoms flip into the (b)-like structure of Figure 9.

The curves indicate that the reaction remains exothermic along all of them and that the energy variations start to be significant only when the relative distance between the two H atoms reaches the structure of the TS complex. The in-plane approach of path 1 also shows a shallow increase before the TS is reached. We have also optimized the angle variation as the H^- anion approaches the molecule and the data in Figure 11 show the small barrier of Figure 10 to be due to the formation of a planar CH_3^- where all three angles now become equal and of 120°. The change in the total energy indicates that no transfer of charge onto the CH_2 partner occurs along this path.

We have further carried out a restricted grid calculation by mapping over the relevant space between the R(H3−H4) and R(H3−C) distances while optimizing at the same time both the θ(H2−C−H3) angle and the R(H2−C) distance.

https://dx.doi.org/10.1021/acs.jpca.0c02412
J. Phys. Chem. A 2020, 124, 5098−5108

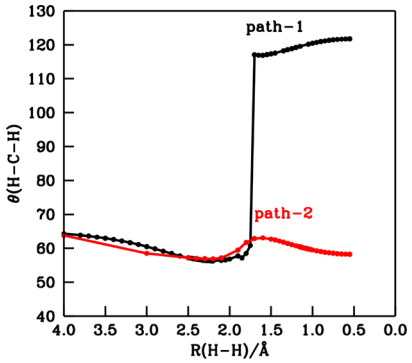

Figure 11. Calculations of the total energy of the complex as a function of the (H2−C−H3) angle as the H^- anion approaches the CH_2 partner. See main text for further comments. The location of the energy jump along path-1 occurs as discussed for Figure 10.

Two different views of this reduced dimensionality reactive PES (RDRPES) are shown in Figures 12 and 13, where the

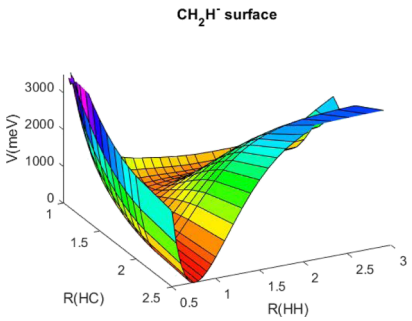

Figure 12. Restricted grid calculations for the RDRPES discussed in the main text. The potential energy curve shown by the front of the surface describes the neutral product H_2 while the curve for the CH^- product is behind the upper asymptote.

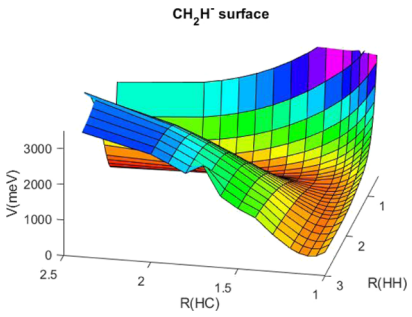

Figure 13. Different view of the MEP configurations along the R(H−H) and the R(C−H) two-dimensional grid. The potential curve shown on the lower right of the surface corresponds to the formation of the CH^- product anion while the neutral H_2 partner product is partly visible on the upper left of the figure. See main text for further discussion.

two regions of product formation are clearly visible, both appearing along an exothermic path without barriers. We therefore suggest that one can use the MEP calculations from this surface as a guide to obtain reaction rates at the expected temperatures in the ISM. This will be discussed in the following section.

3. REACTION RATE COEFFICIENTS

The behavior we have found for the present reaction is very similar to what we have shown in other reactions of astrophysical interest involving H^- and small neutral molecules in refs.[32,34] In those cases, we successfully calculated the rates using the VTST approach. Briefly, the special physical features of this reaction allow us to apply the VTST treatment for temperature-dependent rate constants of exothermic, barrierless reactions.[35] While the TST method searches for a stationary point along the reaction coordinate, the VTST can be applied more generally to reactions that do not have stationary points along their MEPs, although still have a physical point along the MEP where the reaction slows down. The "trajectories" (to use a classical analogy) that are crossing this point are the slowest of all the possible trajectories descending toward the products. Thus, the VTST rate coefficient is obtained by getting the energy minima of the molecular partition functions Q_s along the MEP over a very dense grid of all 3D coordinates, searching the MEP minimum energy in the full dimensionality of all of the reagents' degrees of freedom. The high density of points required needs to use steps of the order of 0.001 Å, followed by a frequency analysis at every point, while the TS theory (TST) calculates the rates from the Q_s of the molecular geometry at the barrier top (stationary point) of the reaction.

Any structure associated to a minimum of its partition function along the MEP exhibits no imaginary frequencies, this being so for those MEP with energies smaller than those of the reactants' entrance channels. Hence, the TS geometry of the VTST is not a stationary point. Thus, all the frequencies are positive even if the MEP has a negative curvature in that region, and all the coordinates along the MEP geometries, except for the reaction coordinate, are simultaneously optimized. On the other hand, the frequency calculations for the TST model require that each element of the second derivative matrix is obtained by fixing all the coordinates except those corresponding to the normal mode. In the standard TST applied to reactions with a barrier, the bottleneck of the "reaction trajectories" is always located exactly at the top of the barrier, where at least one of the frequencies is imaginary. Thus, a difference between VTST and TST treatments is that the former searches for the minima of the Q_s along the MEP structures and includes all the residual degrees of freedom in the optimization steps. It basically assumes the formation of a TS complex along the exothermic energy path from reactants to products, and it further controls the efficiency of product formation via the relative energies between the partition functions of that complex and those of the initial reagents.

This is a type of strong-coupling approximation, where the degrees of freedom within the evolving TS complex are strongly coupled with each other, but because of the low pressure conditions in the ISM environments, there is only a weak coupling with the very diluted, surrounding bath of the other molecules in the ambient. One should note that the collision frequencies with the bath molecules would be much larger than microseconds, while the intramolecular vibrational redistribution (IVR) time scale with the nonreacting degrees of freedom within the Ts would be of the order of 0.1 ps. This time needs to be compared with the time spent by the partners at the TS during the reaction: this may vary from about 150 fs at 300 K to about 350 fs at 10 K. Hence, depending on the

https://dx.doi.org/10.1021/acs.jpca.0c02412
J. Phys. Chem. A 2020, 124, 5098−5108

temperature, the crossing of the MEP during the reaction will occur on a shorter timescale than that of the characteristic IVR rearrangements within the complex.

Thus, once the TS area is reached by the reagents along the MEP, the reactants are in microcanonical equilibrium with their nonreactive surroundings and also with the reactive coordinate and its kinetic and potential energy contents. Under room temperature conditions (i.e., at about 300 K), the TS reactive degree of freedom can then efficiently release its energy (gained during the exothermic process) to the relative kinetic energy of the products while avoiding the transfer of energy to the other nonreactive modes within the complex. Such an assumption could in fact break down when reaction temperatures become much lower than 300 K. This aspect will be discussed in the following.

As a preliminary test, we verify that the generation of several thousands of grid points for the global optimization of all degrees of freedom by the VTST approach can be realistically done by employing the DFT rather than the more costly CCSD(T) treatment. The comparison shown in Figure 14

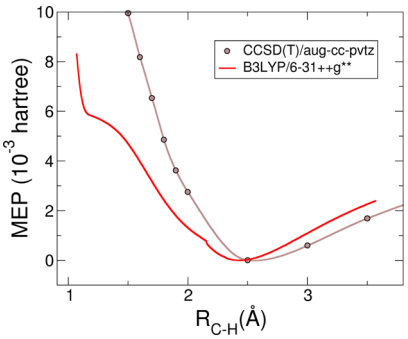

Figure 14. Comparison of the MEP energies obtained around the region of the TS formation. The dots are from the CCSD(T) discussed earlier, and the red line reports the DFT-type of calculation employed for generating the reaction rates discussed in Section 4.

indicates that the location of the TS along the reaction MEP is similarly described by both methods: the two minima are quite near each other because C−H = 2.5 Å with CCSD(T) and C−H = 2.43 Å with B3LYP calculations. Furthermore, the geometry of the variational TS found by the DFT calculations remains essentially constant with T over the examined range of the present study: R(CH3) = 2.32 Å, R(H3−H4) = 0.766 Å, R(C−H2) = 1.143 Å, θ(H2−C−H3) = 177.269 Å. It, therefore, follows that the employment, for computational necessity, of the DFT method to study the present reaction by the VTST approach is going to provide realistic estimates of the required rate constants.

The partition function of the complex, $Q^{\ddagger}_{TS}$, is obtained as the product of the Q_s for the conserved-mode within that complex, $Q^{\ddagger}_{cons}$, times the Q_s of the translational mode

$$Q^{\ddagger}_{TS}(T) = Q^{\ddagger}_{cons}(T)Q^{\ddagger}_{trans}(T) \quad (3)$$

The VTST states that the activation energy is zero, and therefore the exponent of the Arrhenius equation is equal to unity. The pre-exponential factor of the rate coefficient then becomes the only part that needs evaluating to yield reaction rate coefficients $k(T)$. The latter can now be obtained as the ratio between the relevant Q_s of the TS complex and those of all the reagents, as a function of the reaction temperatures

$$k(T) = \frac{k_B T}{h}\frac{Q[(CH_2\cdots H)^-]}{Q[CH_2]Q[H^-]} \quad (4)$$

Here, k_B is the Boltzmann constant and h is the Planck's constant. We obtain at each T the TS geometries at the lowest possible energy along the MEP path (e.g., ref 35). The extra energy acquired by the reactive degree of freedom, as the TS moves exothermically along the MEP toward the products, is efficiently transferred to the relative kinetic energy of the products. Hence, at each temperature, the reaction can proceed in a pseudo−canonical equilibrium within the complex. When the T goes below room values, the rate coefficient is linked to the behavior of the vibrational part of the Q_s for that TS geometry because all other degrees of freedom are now "frozen" to their lowest values in order to satisfy the minimum conditions of the VTST. As the reaction is studied to increasingly lower temperatures, however, the TS's Q_s relate directly to the ZPE values of the considered modes because Q_{vib} (at low T) can be written as: e^{-E_{ZPE}/k_BT}. One should also note at this point that the dense grid of the reactive PES points generated to follow the minima of the partition functions along the IRC coordinate are searching for those minima by sampling fully all the coordinates of the TS geometries. This means that the energetically close-by linear structures of the CH_2 partner are also automatically considered during the calculations and taken into account during the minimization process.

The rate coefficients at low-T are thus linked to changes of the E_{ZPE} values within the Q_s.[32−34] In the present reactions we have: $E^{reacts}_{ZPE} = E^{CH_2}_{ZPE} + E^{H^-}_{ZPE}$ so that we define Δ_{ZPE} as the energy difference between the ZPE of the reactants and that of the TS complex. It controls the slope of the $k(T)$ at low temperatures where the Δ_{ZPE} is most important: a large difference causes a greater decrease of $k(T)$ as T decreases. We computed the minima of the $Q^{\ddagger}_{TS}$ for the TS complex along the computed MEP from reactants to products and found that this minimum is practically coincident with the location of the pseudo-TS along the path already shown in Figure 1. Thus, the reaction step for the ET is located just before the "downhill" path to products that bring the MEP to its absolute minimum.

As usual for reactions of astrochemical interest (e.g., see: ref 36) we have fitted the calculated rate coefficients by using the well-known formula: $k(T) = \alpha(T/300\ K)^{\beta}e^{-\gamma/T}$. The parameters we have obtained are reported in Table 5 below. The data below room temperature have been further scaled according to the procedure explained and discussed in the following section, so that all the data in that table constitute

Table 5. Computed fitting Parameters for the Present Best Estimates of the Reaction Rates over the Three Range of Temperature Examined[a]

T (K)	30−100	100−300	300−1000
α	1.53×10^{-11}	1.36×10^{-11}	8.87×10^{-11}
β	0.22	0.90	2.65
γ	−7.05	−97.04	416.51

[a]The scaled rate coefficients with τ = 5 K has been used for the fitting of the VTST data in the 30−300 K temperature range, while the nonscaled rate coefficients are used for the fitting between 300 and 1000 K. See main text for further comments ($k(T) = \alpha(T/300\ K)^{\beta}e^{-\gamma/T}$). Here α is in $cm^3\ s^{-1}$ and γ in K .

https://dx.doi.org/10.1021/acs.jpca.0c02412
J. Phys. Chem. A 2020, 124, 5098−5108

our best estimate of all the rate constants over the whole range of examined temperatures.

The two panels of Figure 15 report the temperature behavior of the rate coefficients over different ranges of temperatures.

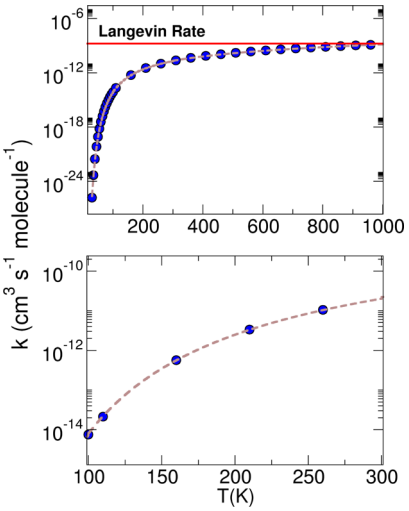

Figure 15. Temperature dependence of the computed VTST rate constants over two different ranges. Top panel: Overall behavior from threshold up to 1000 K. The continuous red line shows the *T*-independent results from the Langevin model; bottom panel: rate behavior from 100 to 300 K. See main text for further discussion.

The top panel further shows the *T*-independent behavior of the Langevin's model. Its value is: 1.702×10^{-9} cm^3 s^{-1} molecule^{-1}. It is interesting to note at this point that the computed rate coefficients are invariably smaller than the Langevin rate, although our VTST computations show that, as the temperature approaches 1000 K, the computed values vary very slowly with *T* and approach the Langevin upper limiting value. The lower panel shows the behavior of the unscaled rate constants (see next subsection) below 300 K.

It is also worth pointing out here that the simple, one-dimensional capture model implied by the Langevin rate constant is really a high-*T* approximation that can be fulfilled when all encounters are fast enough to be able to lead to products irrespective of the details of the nonspherical interaction forces that are guiding the actual collisions. In other words, the physical details of the forces at play are less relevant as *T* increases above about 500 K, and therefore the Langevin limiting value, independent of *T*, is also reached by the computed rate constants, as shown by the upper panel of Figure 15.

The data in the bottom panel show that our computed rate coefficient at 300 K, that is, at room temperature, are of the order of about 4.0×10^{-11} cm^3 s^{-1} molecule^{-1}, indicating that this reaction is expected to be rather efficient when studied at room temperatures. It is interesting to note at this point that our earlier VTST calculations for a similar ionic reaction[34] involving NH_2^- with H_2 and presenting very similar behavior (e.g., markedly exothermic, only a small barrier below the reagents' energy level, nearly collinear TS between reactants) was found experimentally to have a similar value at 300 K, that is, around 3.0×10^{-11} cm^3 s^{-1} molecule^{-1}[37] and, most importantly, to be very accurately predicted by our VTST calculations,[34] with a value of about 3.1×10^{-11} cm^3 s^{-1} molecule^{-1}.[34] Additionally, we have also found that another reaction, that is, the H^- reaction with HCN, yielding CN^- and H_2 in its exothermic channel, was measured in early experiments at 300 K to be of the order of 1.5×10^{-10} cm^3 s^{-1} molecule^{-1}.[37] This experimental value is once more in a very good agreement with our earlier calculations of its rate coefficient at room temperature: (2.0×10^{-10} cm^3 s^{-1} molecule^{-1}).[33] Thus, our earlier studies on similar, but different, systems found that the VTST treatment of the RPES dynamics was correctly reproducing the experimental reaction rate constants at temperatures around 300 K, while however failing to predict experimental rate constants, when existing, at the lower temperatures of more direct astrochemical interest.[34] It is therefore reasonable to expect a similar behavior in the present case, where, unfortunately no experiments are as yet available at any temperature. The corrective procedure that we suggest to employ for the present reaction will be discussed in the following subsection and will be following the scaling scheme already successfully employed in ref 34 to obtain agreement with experiments for its reaction rate coefficients at temperatures well below 300 K.

4. DISCUSSION

The behavior of the present $k(T)$ at low-*T*, given by the lower panel of Figure 15, shows that the large values of the Δ_{ZPE} mentioned earlier (between the geometry of the TS and that of the reagents) is the main reason why one sees the rapid dropping of $k(T)$ as *T* decreases below 300 K. In our earlier study on an exothermic barrierless reaction,[34] we suggested to correct the VTST behavior at $T < 300$ K by scaling the Δ_{ZPE} down to about 10 K using the room-temperature agreement with experiments as a metric for the correct rate constant at 300 K. If a similar behavior is being valid for the present system, we could rewrite the above quantity in a *T*-dependent form

$$\Delta_{ZPE} \Rightarrow \Delta_{ZPE}(T) = \frac{\tau + T}{300\ \text{K}} \cdot \Delta_{ZPE} \tag{5}$$

where τ is a fitting parameter, to which we give here, as an initial guess, the same value of 5.3 K used earlier[34] to give us there agreement with the experiments down to 10 K. We have also used for H_2, CH^-, and CH_2 the quantum formulation of their rotational partition functions as done in ref 34.

As discussed in that work, the role of the extra parameter in eq 4 is essentially that of producing increasingly reduced values of the reaction's Δ_{ZPE} as the temperature decreases. One could say that the $(\tau/300\ \text{K})$ factor in eq 4 describes, in qualitative terms, a small portion of the reaction "trajectories" [the larger portion being given, by $(1 - \tau/300\ \text{K}) = 0.98\%$] which succeeds, as *T* decreases, to transfer the TS acquired excess energy to the relative kinetic energy of the products without heating the nonreactive modes when going below 300 K. This correction should then reduce the flux contributing to obtain the final VTST rate coefficients, only by a controlled amount that still keeps the required pseudo-canonical equilibrium of the VTST complex as the temperature goes down well below room temperature.

The reduced *T*-dependence of the scaled VTST rate constants, as the temperatures reach those of the ISM environments, is shown in Figure 16, where the scaled results from using eq 4 are presented for a range of parameters, close to the value already found to be realistic in our earlier study in ref 34.

The following considerations can be made:

https://dx.doi.org/10.1021/acs.jpca.0c02412
J. Phys. Chem. A 2020, 124, 5098−5108

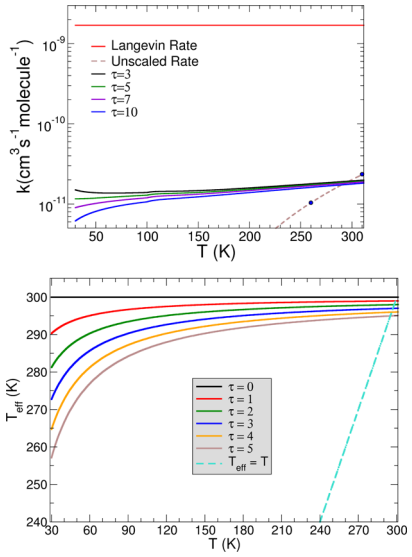

Figure 16. Computed reaction rate coefficients with the scaling parameter defined by eq 4. The upper panel shows also the Langevin value (red line) and the upper range of the unscaled results given in previous figure (dotted line). The lower panel presents the dependence of the T_{eff} values on the choice of the τ parameter as a function of the physical temperature T. See main text for further discussion. τ is in units of K.

- for exothermic reactions below room temperatures, we have argued earlier that the TS structure is not capable of keeping its thermal balance with the other degrees of freedom during the MEP crossing of the reaction region, where the usual formulation of the VTST fails.
- our scaling procedure suggests a way to reduce the flux contributing to the final VTST rate coefficients so that it holds the required pseudo-canonical equilibrium of the TS complex as the reaction goes increasingly below 300 K.
- we have already pointed out before that the VTST model is able to find good agreement with experiments at 300 K in other ion−molecule reactions involving H^-, as in the present case. Our scaling therefore fixes the rate constant at room temperature and employs a range of τ scaling values, which, in earlier choices, have provided good agreement with existing low-T experiments.[34]

The data in the two panels of Figure 16 indicate clearly that how the scaled rate constants reach a set of values around 10^{-11} cm^3 s^{-1} $molecule^{-1}$, which is fairly close to the value found experimentally by the similar exothermic reaction of ref 34 around 50 K;

- the scaled values of the rate coefficients now show a slow dependence on T in the range examined by Figure 16. This slow dependence is also in agreement with earlier results on similar systems: it indicates that the corrected TS behavior now follows more realistic trends, which are more in line with existing experiments on similar systems;
- to deepen the understanding of the role of the parameter τ, one could link it to an effective temperature for the TS in its path along the MEP. This temperature would be distinct from its true temperature whenever the reaction goes below 300 K: $T_{eff} = 300\ K \times T/(\tau + T)$.

We see that, for the temperatures below 300 K, the T_{eff} indicates that the reactive system partially heats the non-reactive modes because the TS complex now spends more time along the MEP. To compensate for this shortcoming, the T_{eff} value has to become larger than the actual physical temperature of the bath of reagent molecules, thereby accelerating the passage of the reacting partners along the MEP. As one moves closer to 300 K, the T_{eff} essentially matches the correct physical temperature of the reaction as the VTST model follows the MEP path and the process reaches a pseudo-canonical situation, its energy now equal to the Boltzmann's value at room temperatures.

To pictorially show what this temperature scaling means in terms of different τs within the range suggested by the previous scaling procedure, we show in the lower panel of Figure 16 the relationship between that parameter and the T_{eff} at the different physical temperatures. One can see that the values around 5 K introduce in the low-T range a much higher effective temperature for the partners crossing the MEP at the TS geometries. It shows that the VTST model can be corrected at temperatures below room temperature to achieve a more efficient equilibration of the Q_s of the TS complex during the minimization procedure.

5. CONCLUSIONS

We have analyzed in the present study the structural features and the overall energetics for an ion−molecule reaction of possible interest in the chemistry of the ISM, specifically to models of the chemical networks considered to be in the atmosphere of Titan. This reaction is driven by the presence of H^- anions reacting with CH_2 molecules to form another C-bearing molecular anion: the CH^- as the smallest term in the anionic polyenes discussed in those chemical networks.[21]

The reaction 1 is shown to be markedly exothermic, with only a shallow barrier to the formation of the TS complex along the MEP coordinate, and occurring within a nearly collinear path of approach of H^- to one of the CH_2 bonds. That same path also reaches the ET step for the formation of the final CH^- anion. We have employed the VTST approach to obtain the reaction rate coefficients from T around 1000 K down to 300 K, and further down to the lower temperatures, which are present within the Titan's environment or in the inner regions of the dark molecular clouds. The VTST approach had already provided rate coefficients in good accord with the existing experiments with H^- at temperatures around 300 K and involving similar molecular partners (e.g., see: refs[32,34]). Hence, we stipulate in the present study that the VTST rate obtained here at that temperature could be used as a metric to scale the reaction rate constants well below 300 K.

The scaling was carried out by selecting a parameter τ, which simulates below 300 K an effective higher temperature for the TS partition functions as the reaction complex is crossing the MEP region. This scaling correctly allows the TS complex to reach a pseudo-canonical equilibrium with the residual degrees of freedom in the reaction bath, thereby restoring the required VTST conditions of minimum energy for its partition functions along its way to products.

The final results indicate that the reaction becomes close to the Langevin upper limit when T is around 1000 K, it decreases below that limit when going down to room temperature, and further reaches rate coefficient values around 10^{-11} cm^3 s^{-1} $molecule^{-1}$ when the temperature descends to

https://dx.doi.org/10.1021/acs.jpca.0c02412
J. Phys. Chem. A 2020, 124, 5098−5108

the 30 K region expected to be present in the astrochemical environments described in the Introduction.

In conclusion, the possibility that the present reaction could play a role in the destruction of CH_2 molecules via their interaction with H^- anions in the chemistry of Titan's atmosphere is seen from the present investigation to be a possibility worth including in larger kinetics models, a conclusion that should encourage new laboratory investigations of this reaction to obtain realistic experimental data for this process.

AUTHOR INFORMATION

Corresponding Author

F. A. Gianturco − *Institut für Ionen Physik und Angewandte Physik, Leopold-Franzens-Universität, 6020 Innsbruck, Austria;* orcid.org/0000-0003-3962-530X; Email: francesco.gianturco@uibk.ac.at

Authors

E. Yurtsever − *Department of Chemistry, Koc University, 34450 Istanbul, Turkey;* orcid.org/0000-0001-9245-9596

M. Satta − *CNR-ISMN and Department of Chemistry, The University of Rome Sapienza, 00185 Rome, Italy*

R. Wester − *Institut für Ionen Physik und Angewandte Physik, Leopold-Franzens-Universität, 6020 Innsbruck, Austria;* orcid.org/0000-0001-7935-6066

Complete contact information is available at: https://pubs.acs.org/10.1021/acs.jpca.0c02412

Notes

The authors declare no competing financial interest.

ACKNOWLEDGMENTS

F.A.G. and R.W. acknowledge the financial support by the Austrian Science Fund (FWF), Project I2920-N27.

REFERENCES

(1) Dalgarno, A.; McCray, R. A. The Formation of Interstellar Molecules from Negative Ions. *Astrophys. J.* **1973**, *181*, 95−100.

(2) Herbst, E. Can Negative Molecular Ions be Detected in Dense Interstellar Clouds? *Nature* **1981**, *289*, 656−657.

(3) Carelli, F.; Satta, M.; Grassi, T.; Gianturco, F. A. Carbon-rich Molecular Chains in Protoplanetary and Planetary Atmospheres: Quantum Mechanisms and Electron Attachment Rates for Anion Formation. *Astrophys. J.* **2013**, *774*, 97.

(4) McCarthy, M. C.; Gottlieb, C. A.; Gupta, H.; Thaddeus, P. Laboratory and Astronomical Identification of the Negative Molecular Ion C_6H^-. *Astrophys. J.* **2006**, *652*, L141.

(5) Sakai, N.; Sakai, T.; Osamura, Y.; Yamamoto, S. Detection of C_6H^- Toward the Low-mass Protostar IRAS 04368+2557 in L1527. *Astrophys. J.* **2007**, *667*, L65.

(6) Remijan, A. J.; Hollis, J. M.; Lovas, F. J.; Cordiner, M. A.; Millar, T. J.; Markwick-Kemper, A. J.; Jewell, P. R. Detection of C_8H^- and Comparison with C_8H Toward IRC +10216. *Astrophys. J.* **2007**, *664*, L47.

(7) Cernicharo, J.; Guélin, M.; Agúndez, M.; Kawaguchi, K.; McCarthy, M.; Thaddeus, P. Astronomical Detection of C_4H^-, the Second Interstellar Anion. *Astr. Astrophys.* **2007**, *467*, L37−L40.

(8) Cernicharo, J.; Guélin, M.; Agúndez, M.; McCarthy, M. C.; Thaddeus, P. Detection of C_5N^- and Vibrationally Excited C_6H in IRC +10216. *Astrophys. J.* **2008**, *688*, L83.

(9) Agúndez, M.; Cernicharo, J.; Guélin, M.; Kahane, C.; Roueff, E.; Kłos, J.; Aoiz, F. J.; Lique, F.; Marcelino, N.; Goicoechea, J. R.; et al. Astronomical Identification of CN^-, the Smallest Observed Molecular Anion. *Astr. Astrophys.A&A* **2010**, *517*, L2.

(10) Millar, T. J.; Herbst, E.; Bettens, R. P. A. Large Molecules in the Envelope Surrounding IRC+10216. *Monthl. Notic. Royal Astron. Soc.* **2000**, *316*, 195−203.

(11) Millar, T. J.; Walsh, C.; Cordiner, M. A.; Ní Chuimín, R.; Herbst, E. Hydrocarbon Anions in Interstellar Clouds and Circumstellar Envelopes. *Astrophys. J.* **2007**, *662*, L87.

(12) Harada, N.; Herbst, E. Modeling Carbon Chain Anions in L1527. *Astrophys. J.Astrophysical Journal* **2008**, *685*, 272.

(13) Best, T.; Otto, R.; Trippel, S.; Hlavenka, P.; von Zastrow, A.; Eisenbach, S.; Jézouin, S.; Wester, R.; Vigren, E.; Hamberg, M.; Geppert, W. D. Absolute Photodetachment Cross-section Measurements for Hydrocarbon Chain Anions. *Astrophys. J.* **2011**, *742*, 63.

(14) Kumar, S. S.; Hauser, D.; Jindra, R.; Best, T.; Roučka, Š.; Geppert, W. D.; Millar, T. J.; Wester, R. Photodetachment as a Destruction Mechanism for Cn-and C3N-anions in Circumstellar Envelopes. *Astrophys. J.* **2013**, *776*, 25.

(15) Yang, Z.; Cole, C. A.; Martinez, O., Jr; Carpenter, M. Y.; Snow, T. P.; Bierbaum, V. M. Experimental And Theoretical Studies Of Reactions Between H Atoms And Nitrogen-Containing Carbanions. *Astrophys. J.* **2011**, *739*, 19.

(16) Wang, Z.-C.; Cole, C. A.; Demarais, N. J.; Snow, T. P.; Bierbaum, V. M. Reactions of Azine Anions with Nitrogen and Oxygen Atoms: Implications for Titan's Upper Atmosphere and Interstellar Chemistry. *J. Am. Chem. Soc.* **2015**, *137*, 10700−10709.

(17) Leopold, D. G.; Murray, K. K.; Miller, A. E. S.; Lineberger, W. C. Methylene: A Study of the X^3B_1 and a^1A_1 States by Photoelectron Spectroscopy of CH_2 and CD_2. *J. Chem. Phys.* **1985**, *83*, 4849.

(18) Bunker, P. R.; Sears, T. J. Analysis of the Laser Photoelectron Spectrum of CH_2^-. *J. Chem. Phys.* **1985**, *83*, 4866.

(19) Martinez, O.; Yang, Z.; Demarais, N. J.; Snow, T. P.; Bierbaum, V. M. Gas-Phase Reactions Of Hydride Anion H^-. *Astrophys. J.* **2010**, *720*, 173.

(20) Walsh, C.; Harada, N.; Herbst, E.; Millar, T. J. The Effects of Molecular Anions on the Chemistry of Dark Clouds. *Astrophys. J.* **2009**, *700*, 752.

(21) Vuitton, V.; Lavvas, P.; Yelle, R. V.; Galand, M.; Wellbrock, A.; Lewis, G. R.; Coates, A. J.; Wahlund, J.-E. Negative ion chemistry in Titan's upper atmosphere. *Planet. Space Sci.* **2009**, *57*, 1558.

(22) Ziurys, L. M. The chemistry in circumstellar envelopes of evolved stars: Following the origin of the elements to the origin of life. *Proc. Natl. Acad. Sci.* **2006**, *103*, 12274.

(23) Chase, M. J. NIST-JANAF Themochemical Tables, Fourth Edition. *J. Phys. Chem. Ref. Data* **1951**, *9*, 1.

(24) Shiell, R. C.; Hu, X.; Hu, i. J.; Hepburn, J. W. Threshold Ion-pair Production Spectroscopy (TIPPS) of H_2 and D_2. *Faraday Disc.* **2000**, *115*, 331.

(25) *CODATA Key Values for Thermodynamics*; Hemisphere Publishing Corp.: New York, 1984.

(26) Prasad, S. S.; Huntress, W. T. J., Jr. A model for gas phase chemistry in interstellar clouds. I - The basic model, library of chemical reactions, and chemistry among C, N, and O compounds. *Astrophys. J. Suppl. Ser.* **1980**, *43*, 1.

(27) Werner, H.-J.; Knowles, P. J.; Knizia, G.; Manby, F. R.; Schütz, M. Molpro: A General-purpose Quantum Chemistry Program Package. *WIREs Comput. Mol. Sci.* **2012**, *2*, 242−253.

(28) Frisch, M. J.; Trucks, G. W.; Schlegel, H. B.; Scuseria, G. E.; Robb, M. A.; Cheeseman, J. R.; Scalmani, G.; Barone, V.; Petersson, G. A.; Nakatsuji, H.; et al. Gaussian 09, **2009**, Revision E.01 gaussian Inc. Wallingford CT (USA).

(29) Goebbert, D. J. Photoelectron Imaging of CH^-. *Chem. Phys. Lett.* **2012**, *551*, 19.

(30) Fukui, K.; Kato, S.; Fujimoto, H. Constituent Analysis of the Potential Gradient Along a Reaction Coordinate. Method and an Application to Methane + tritium Reaction. *J. Am. Chem. Soc.* **1975**, *97*, 1.

(31) Ishida, K.; Morokuma, K.; Komornicki, A. The Intrinsic Reaction Coordinate. An Ab Initio Calculation for HNC^- + *HCN* and H^- + CH_4 = CH_4 + H^-. *J. Chem. Phys.* **1977**, *66*, 2153.

(32) Gianturco, F. A.; Satta, M.; Mendolicchio, M.; Palazzetti, F.; Piserchia, A.; Barone, V.; Wester, R. Exploring a Chemical Route For The Formation of Stable Anions of Polyynes C_nH^- (n=2, 4) in Molecular Clouds. *Astrophys. J.* **2016**, *830*, 2.
(33) Satta, M.; Gianturco, F. A.; Carelli, F.; Wester, R. A Quantum Study of the Chemical Formation of Cyano Anions in Inner Cores and Diffuse Regions of Interstellar Molecular Clouds. *Astrophys. J.* **2015**, *799*, 228.
(34) Gianturco, F. A.; Yurtsever, E.; Satta, M.; Wester, R. Modeling Ionic Reactions at Interstellar Temperatures: The Case of $NH_2^-+H_2\leftrightarrow NH_3+H^-$. *J. Phys. Chem. A* **2019**, *123*, 9905.
(35) Fernández-Ramos, A.; Miller, J. A.; Klippenstein, S. J.; Truhlar, D. G. Modeling the Kinetics of Bimolecular Reactions. *Chem. Rev.* **2006**, *106*, 4518. , and references quoted therein
(36) Gianturco, F. A.; Satta, M.; Yurtsever, E.; Wester, R. Formation of Anionic C, N- bearing Chains in the Interstellar Medium via Reactions of H^- with HC_xN for Odd- valued x from 1 to 7. *Astrophys. J.* **2017**, *850*, 42.
(37) Otto, R.; Mikosch, J.; Trippel, S.; Weidemueller, M.; Wester, R. Nonstandard Behavior of a Negative Ion Reaction at Very Low Temperatures. *Phys. Rev. Lett.* **2008**, *101*, 063201.

https://dx.doi.org/10.1021/acs.jpca.0c02412
J. Phys. Chem. A 2020, 124, 5098−5108